FACTA UNIVERSITATIS
Series: **Mechanical Engineering**
https://doi.org/10.22190/FUME210722066T

Original scientific paper

APPLICATION POSSIBILITIES OF THE S960 STEEL IN UNDERWATER WELDED STRUCTURES

Jacek Tomków, Michał Landowski, Grzegorz Rogalski

Faculty of Mechanical Engineering and Ship Technology, Gdańsk University of Technology, Poland

Abstract. *In this paper, the application possibilities of the ultra-high strength (UHSS) Domex 960 steel in the underwater welded structures are analyzed. In the research, the investigated material has been tested in bead-on-plate wet welding conditions with the usage of different heat input values, namely 0.63 kJ/mm, 0.72 kJ/mm and 0.93 kJ/mm. Specimens were performed by the manual metal arc (MMA) welding method with the usage of rutile covered electrodes. Firstly, the nondestructive visual testing (VT) was carried out. In the next step, the metallographic macro- and microscopic tests were performed. Finally, the hardness of the weld metal and heat-affected zone (HAZ) was measured by the Vickers HV10 method. The performed experiments allow the statement that the Domex 960 steel could be welded in a water environment. It also showed that increasing heat input leads to decreasing the hardness in HAZ by 30 HV10. It may result in decreasing the susceptibility to cold cracking during butt- and filet welding in the water environment.*

Key Words: *Underwater Welding, Ultra-high Strength Steel, Microstructure, Macroscopic Testing, Hardness Measurements, Cold Cracking*

1. INTRODUCTION

Underwater welding is a special process, which requires special equipment or high-qualified welders. Underwater processes could be classified in three groups. Dry welding allows us to isolate the welding area and welder from the surrounding environment by locating them in a special chamber [1]. The biggest limitation of this method is a high cost of the chamber. Following this, it is used only for building underwater structures, e.g., pipelines. Another underwater welding method is local cavity welding [2]. It uses a small

Received July 22, 2021 / Accepted October 23, 2021
Corresponding author: Jacek Tomków
Faculty of Mechanical Engineering and Ship Technology, Gdańsk University of Technology, Gabriela Narutowicza 11/12 street, 80-233 Gdańsk, Poland
E-mail: jacek,tomkow@pg.edu.pl

chamber, which isolates the welding arc and molten metal from the water environment. However, the welding equipment and welder diver are located directly in the water [3,4]. While using this method, the welding area is covered by the chamber. Following this, there are problems with controlling the process, which is the biggest disadvantage of local cavity welding. The third and most used method is wet welding [5]. In wet welding, the welder diver and the whole welding area are in direct contact with water. It is mostly carried out by Manual Metal Arc (MMA) welding [6,7] and Flux Cored Arc Welding (FCAW) [8,9]. Wet welding is the most often used underwater welding method, due to cheaper and smaller equipment.

Water generates some problems during welding. Firstly, it creates water bubbles near the welding arc, which leads to limited visibility [10]. This makes it difficult for welders to control the process [11]. Another problem is instability of the welding arc, which decreases the quality of the performed joints [12,13]. Furthermore, water provides slag inclusions in the weld metal, which decrease the mechanical properties of welded structures [14]. The next problem generated by water is high diffusible hydrogen content in the deposited metal, which is one of the factors responsible for the cracking of steel-welded joints [15]. Fydrych and Łabanowski [16] showed that a water environment generates at least two times higher amounts of hydrogen than during welding in air. Klett et al. [17] performed investigations, which showed that no significant differences in the diffusible hydrogen content could be found between the samples of varying geometry. This amount depends on the used materials. One of the underwater welding problems is the increased cooling rate. A high cooling rate generates brittle microstructures in heat-affected zone (HAZ) [18]. Mentioned factors are responsible for high susceptibility to cold cracking of steel during welding in a water environment [19]. Cracking phenomenon leads to decreasing the weldability in wet welding conditions, which is the reason of the poor quality of welded structures [20].

Offshore steel structures in marine environment face a high degree of damage due to dynamic environmental and operational factors such as corrosion, fatigue cracking, or cold cracking [16,18,21,22]. Many repairs have to be performed in the water environment [23]. Underwater repair processes have been described for mild steels and high-strength low-alloy steels [7,11,20]. However, for offshore structures, ultra-high strength steels (UHSS) are used increasingly each year [24]. Their behavior during underwater welding has not been investigated earlier. The literature analysis showed that there are some problems with welding the S960 UHSS in the air, which is popular as a material for offshore structures. Welded joint parameters and microstructural characterization strongly depend on the parameters of a welding process [25,26]. Improper parameters lead to angular distortion of the joint [27], form brittle structures in the HAZ [28] and form welding imperfections [29,30]. Mician et al. [31] focused on the influence of the cooling rate on the mechanical properties of the joints. They showed that a lower cooling rate leads to decreasing the yield point and tensile strength of S960 steel joints. Similar results were observed by Szymczak et al. [32]. It was stated that micro-jet cooling, which increases the cooling rate, leads to improve the mechanical properties of welded joints. It suggests that this material may be welded in a water environment, where the cooling rate is very high. However, the S960 steel is characterized by high susceptibility to hydrogen-assisted cracking [33]. Schaupp et al. [34] demonstrated that cracks occur in the coarse-grained HAZ. This area of cracking is typical for underwater processes [16,18].

Furthermore, Schaupp et al. [35] in their next paper showed that S960 UGSS is characterized by a high risk for hydrogen-assisted cracking both in the weld metal and in the HAZ. These investigations suggest that the S960 steel may be characterized by very high susceptibility to cold cracking in underwater conditions, due to a high amount of water during joining in this environment.

However, the behavior of UHSS during wet welding has not been investigated yet. The aim of the presented research was to assess the possibility of welding the S960 steel in wet welding conditions. Moreover, the influence of heat input on the microstructure and hardness in different areas of underwater welded structures were investigated.

2. Materials and Methods

2.1 Materials

As a material for the experiment, S960 thermomechanically rolled steel plates with dimensions of 150×100×6 mm were chosen. There is a lack of filler material for welding in water for the materials with grade S960. However, the common E42 2 1Ni RR 51 covered electrodes (4.0 mm diameter) for underwater welding were selected. The chemical compositions of the used materials are presented in Table 1, and their mechanical properties are shown in Table 2. Presented values are in accordance with the manufacturer data.

Table 1 Chemical composition of used materials, wt. %

Material	C	Si	Mn	Cr	S	P	Ni	Al	Carbon equivalent Ce_{IIW}
S960 steel	0.18	0.50	2.1	17.57	0.010	0.020	-	0.018	0.50
E42 2 1Ni RR 51 electrode	0.05	0.45	0.5	19.00	0.025	0.025	0.3	-	-

Table 2 Mechanical properties of used materials

Material	R_e [MPa]	R_m [MPa]	A_5 [%]
S960 steel	min. 960	960-1250	min. 8
E42 2 1Ni RR 51 electrode deposit	-	min. 540	min. 10

2.2 Methods

The welding process was performed manually using the MMA process. Three specimens were bead on plate welded in tap water (20 °C) at 0.25 m depth in the flat position (PA). Each specimen was prepared by laying one bead in the middle of the plate. For welding, the negative (DC-) polarity was used following the filler material manufacturer requirements. Welding parameters such as welding current (I) and arc voltage (U) were selected in the range required by the covered electrode manufacturer. The welding speed (Vsp) was chosen to obtain different heat input (ql) values to show the

influence of heat input on the properties of wet welded specimens. Welding parameters are presented in Table 3.

Table 3 Welding parameters

Specimen	I [A]	U [V]	Vsp [mm/s]	ql [kJ/mm]
1	196	26.8	8.34	0.63
2	220	28.8	8.80	0.72
3	232	30.5	7.54	0.93

After welding, each specimen was subjected to nondestructive and destructive testing. Firstly, the visual test (VT) following the EN ISO 17637:2017 standard was performed. This test started 48 h after welding, which is necessary to avoid cold cracks after VT. Secondly, the specimens were cut, ground, polished, and etched (Nital 4 %) for destructive testing. The metallographic macro- and microscopic tests were performed in accordance with EN ISO 17639:2013 standard. Macrographs were taken using a Canon EOS 1200D camera. For microscopic investigations, the Olympus BX51 light microscope was used. In the last step, the Vickers HV10 hardness measurements were performed. Hardness was measured in the measurement line following Fig 1. This line was located in the axis of the weld bead.

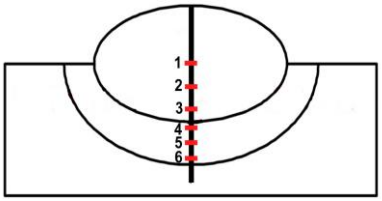

Fig. 1 Schematic view of hardness measurement points distribution

3. Results and Discussion

3.1 Visual testing

The main aim of VT was choosing areas without imperfections, from which the samples were cut for further investigations. Results of VT are shown in Fig. 2. During welding, some problems typical for wet welding were observed. During Specimen 1 performing, there was a problem with burning the welding arc. However, after burning, the arc was stable, and no further problems occurred. The geometry of the performed bead was satisfactory (Fig. 2a). Sample for further investigations was cut in the middle of the bead. There was no problem with initiating the process in Specimen 2. However, the instability of the welding arc was observed near the beginning of the bead (green arrow in Fig. 2b). Moreover, the shape defects were detected in the middle of the sample (red arrow in Fig. 2b). The sample for further investigations was cut from an area without

imperfections. No problems were observed during the Specimen 3 preparation. The welding arc was stable. No serious imperfections were detected during VT (Fig. 2c). Moreover, the welds showed differences due to different heat input. The narrow weld morphology can be observed for specimen welded with the lowest heat input (Fig. 2a). With the increase of heat input, the weld size continues to become wider. Similar results were observed by Wang et al. [36] and Tomków et al. [37].

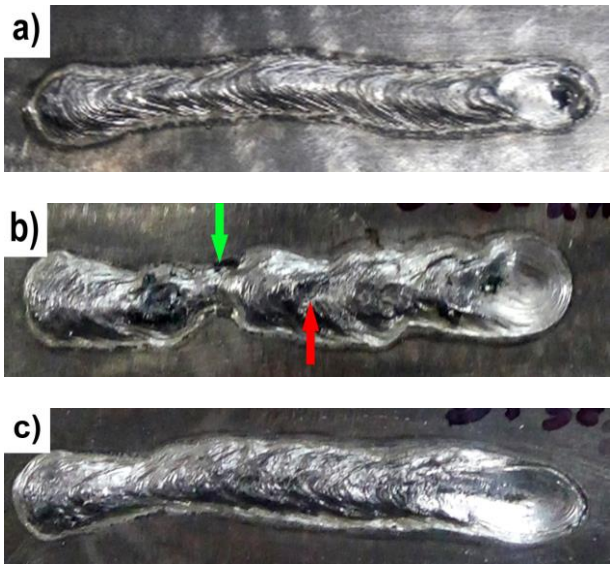

Fig. 2 Results of VT; a) Specimen 1, b) Specimen 2 – results of instability of welding arc (green arrow), shape defects (red arrow), c) Specimen 3

3.2 Macroscopic testing

The exemplary results of the macroscopic test are presented in Fig. 3. Performed investigations showed a significant influence of welding heat input on the size of HAZ. Increasing heat input leads to increasing the area of HAZ. Similar results were observed for underwater wet welding of S700MC steel [37]. Moreover, in Specimen 3 (Fig. 3c) the coarse-grained HAZ is the widest, which may result in microcracks typical for welding in the water environment [11,20]. Besides assessing the HAZ size, macroscopic tests were carried out to detect welding imperfections. In Specimen 1 two cracks were observed (Fig. 3a). These cracks run through the HAZ perpendicularly to the fusion line. It suggests that the heat input (0.63 kJ/mm) is too low for the S960 UHSS welding. Macroscopic test of Specimen 2 confirmed results of VT. The shape defect of the performed bead was observed (Fig. 3b). However, no other imperfections were detected. In Specimen 3, no macrocracks were observed (Fig. 3c), but an undercut was detected. This imperfection is typical for a high value of heat input, which was demonstrated by Tomków et al. [37,38]. The macroscopic tests showed differences in weld geometries in different specimens. It can be seen that the weld width, weld penetration, and weld reinforcement approximately increase with increasing the heat input.

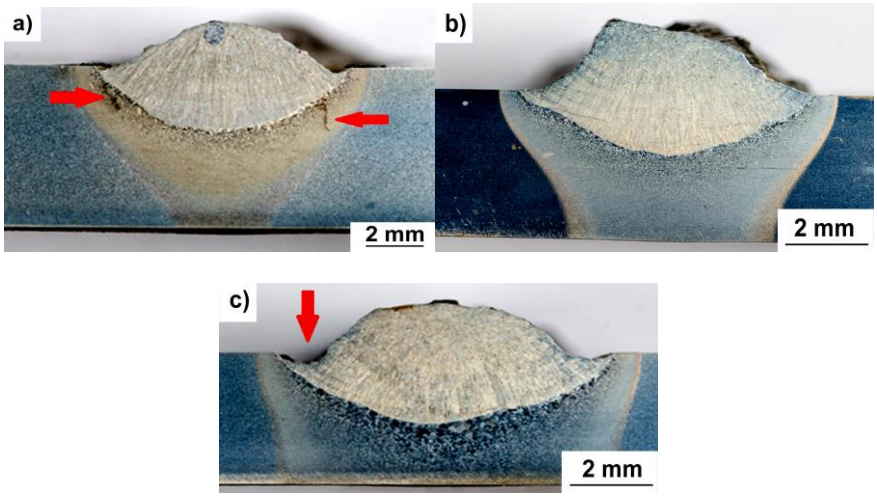

Fig. 3 Exemplary macrographs; a) Specimen 1 – cracks in HAZ, b) Specimen 2, c) Specimen 3 - undercut

3.3 Microscopic testing

The exemplary photographs of the investigated microstructures are shown in Fig. 4. During metallographic microscopic tests, the weld metal areas and HAZ of each specimen were observed. Moreover, the base metal (BM) was investigated. BM is characterized by fine-grained bainitic-martensitic microstructure. The photos of the microstructure in the weld metal showed a typical dendritic structure (Fig. 4a, 4c and Fig. 4e). Dendrites are arranged with columns. They rise to the axis of the performed bead. The microstructure of the weld metal consists of a mixture of bainitic and martensitic phases. With increasing the heat input, the content of martensite slightly increased. Similar results were observed earlier by Schaupp et al. [34]. More differences were observed in HAZ for different specimens. Specimen 1 welded with the lowest value of the heat input presented in the HAZ mostly coarse-grained martensitic microstructure near the fusion line, with a small amount of bainite (Fig. 4b). With increasing the heat input value, the content of bainite also increased (Fig. 4d and 4f). The width of HAZ increased with increasing heat input. It confirms the results of macroscopic observations. In the area of HAZ located near the BM, the partially tempered region with a bainitic-ferritic structure may be observed (Fig. 4d). Kurc-Lisiecka and Lisiecki [39] observed the same effect during laser welding of Domex 960 steel. However, the width of HAZ in their specimens was much smaller than during underwater welding.

Microscopic observations also showed the influence of heat input on the number of cracks in the HAZ. As well as in the macroscopic tests, the biggest number of cracks was found in Specimen 1, welded with the lowest heat input. Except the two long cracks detected in macroscopic investigations (Fig. 3a), the HAZ consists of many short cracks parallel to the fusion line (Fig. 4b). The location of the presented cracks is typical for underwater welding [11]. Wang et al. [40] showed that low heat input values of high-strength steel in underwater conditions lead to an increased number of cracks. It was

stated that the investigated materials should be welded with a higher heat input, which allows decreasing of the susceptibility to cracking. A lower number of cracks were found during Specimen 3 observations. In this specimen, the cracks were located in the coarse-grained region of HAZ and run perpendicularly to the fusion line (Fig. 4f). Unexpectedly, the lowest number of cracks was found in Specimen 2. No cracks were observed in coarse-grained HAZ. However, a long crack (800 μm) was found in the region of HAZ, located near the BM (Fig. 4d).

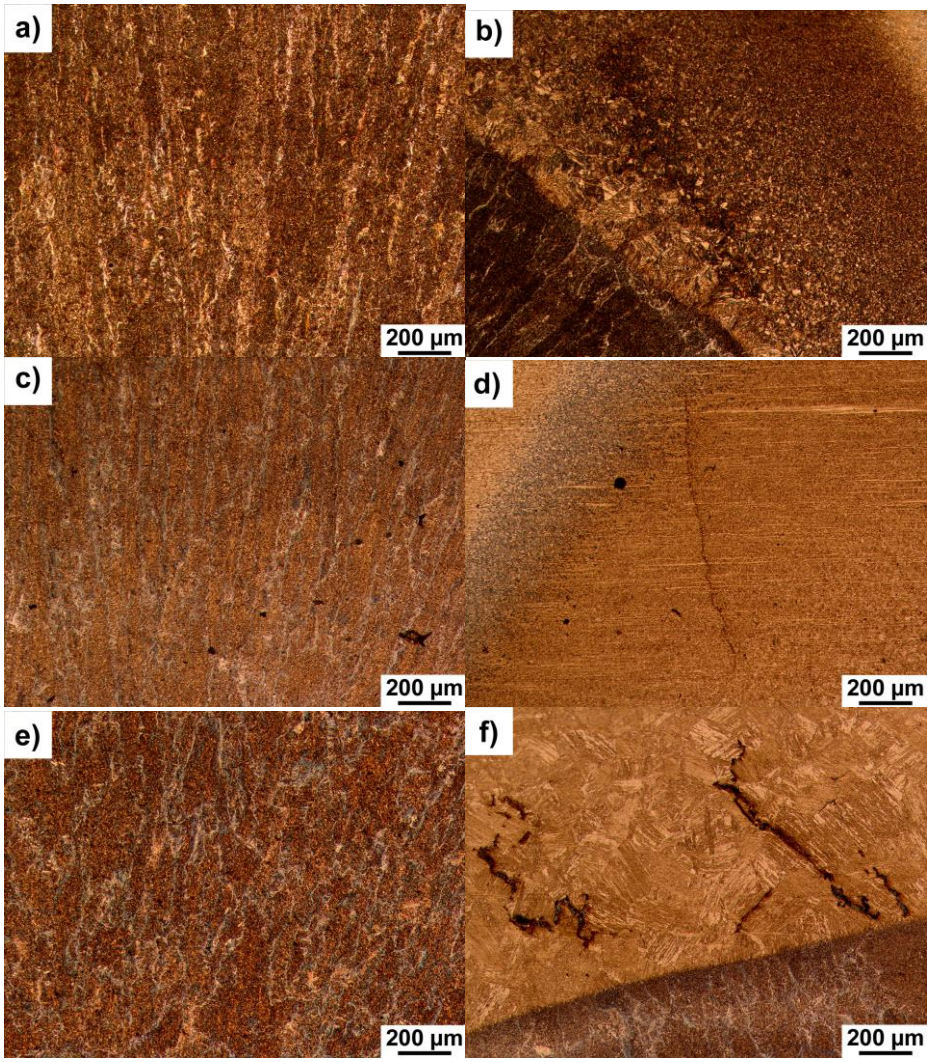

Fig. 4 Exemplary micrographs; a) Specimen 1 – weld metal, b) Specimen 1 - HAZ, c) Specimen 2 – weld metal, d) Specimen 2 – HAZ, e) Specimen 3 – weld metal, f) Specimen 4 - HAZ

3.4 Hardness measurements

Results of Vickers HV10 hardness measurements are presented in Fig. 5. Before the measurements following scheme (Fig. 1), the Domex 960 UHSS hardness was measured. It was in the range 330-350 HV10. In the next step, the hardness in different regions was measured in each specimen. No significant influence of the heat input value on the weld metal hardness was observed. All measurements were in the range of 262-283 HV10. The hardness in HAZ was higher than the weld metal hardness for all cases, which is typical for welding steels characterized by high-strength [11,37,40]. Performed measurements showed a strong relationship between heat input value and HAZ hardness. It was observed that increasing heat input leads to decreasing the HAZ hardness. The highest values were found in Specimen 1, which was welded with the lowest heat input (0.63 kJ/mm). Values significantly exceeded 400 HV10 (the highest 448 HV10), and decreased with the distance from the fusion line, which was observed for each specimen. In other specimens, each measurement was lower than 400 HV10. The lower values were observed in Specimen 3 welded with 0.93 kJ/mm. However, microscopic tests showed that this specimen was characterized by the cracks presence in the HAZ. It suggests that heat input 0.93 kJ/mm may be too high during welding and can lead to failure of underwater wet welded structures. The lowest hardness in specimen welded with the highest heat input confirmed the results of microscopic tests. The HAZ of Specimen S3 consists of a higher content of bainitic microstructure, which is characterized by lower hardness than martensite [37].

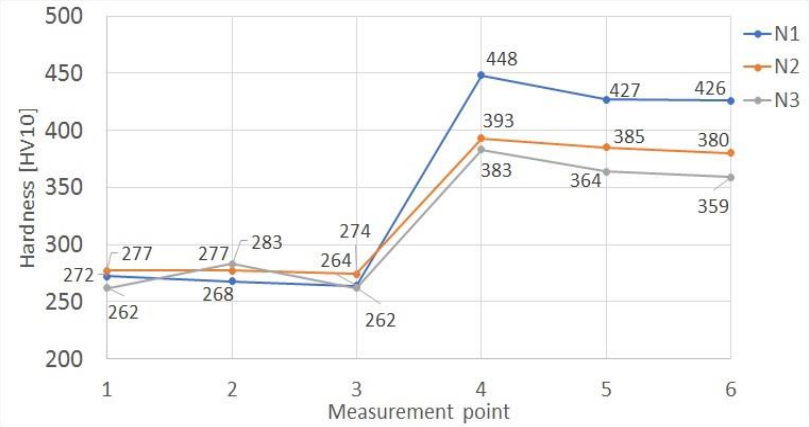

Fig. 5 Results of Vickers HV10 measurements, N1 – 0.63 kJ/mm, N2 – 0.72 kJ/mm, N3 – 0. 93 kJ/mm

5. CONCLUSIONS

In the paper, the application possibility of the Domex 960 steel in underwater welded structures was assessed. The assessment was prepared by testing bead on plate welded structures performed with different heat input values. Investigations showed a significant influence of welding parameters on the properties and microstructure of wet welded

structures made by UHSS. It was showed that the Domex 960 steel may be considered for underwater welding. However, the heat input values must be carefully controlled. The main conclusions resulting from the experiments are:

1. The investigated Domex 960 ultra-high strength steel may be welded in underwater conditions by covered electrodes. However, there is a range of heat input, which leads to formation cracks in the HAZ. The lowest number of cracks was found during welding with 0.72 kJ/mm heat input.
2. Performed measurements showed a strong relationship between heat input value and HAZ hardness. It was observed that increasing the heat input allows decreasing the hardness in the HAZ by 60-70 HV10. The lowest hardness was found in the specimen welded with 0.93 kJ/mm. However, this value leads to forming cracks in the HAZ. The highest number of cracks was found in the specimen performed with the lowest 0.63 kJ/mm heat input.
3. As a reference range of heat input during welding, the Domex 960 UHSS values between 0.7 and 0.9 kJ/mm may be used. These values allow decreasing the hardness in the HAZ after welding. Moreover, the number of cracks occurring in structures welded with these parameters is much smaller than during welding with different heat inputs.
4. Performed investigations are the first, in which the 960 MPa grade steel was welded in underwater wet welding conditions. To confirm the possibility to perform underwater welded structures with the mentioned materials, additional tests should be done: weldability tests (Tekken and CTS), and investigation of the use of the temper bead welding (TBW) technique in wet welding conditions.

REFERENCES

1. Sun, K., Hu, Y., Shi, Y., Liao, B., 2020, *Microstructure evolution and mechanical properties of underwater dry welded metal of high strength steel Q690E under different water depths*, Polish Maritime Research, 27, pp. 112-119.
2. Cheng, Q., Guo, N., Fu, Y., Zhang, D., Wang, G., Yu, M., 2021, *Underwater wire-feed laser deposition of thin-Walled tubular structure of aluminum alloy*, Journal of Manufacturing Processes, 67, pp. 56-62.
3. Cui, S., Xian, Z., Shi, Y., Liao, B., Zhu, T., 2019, *Microstructure and impact toughness of local-dry keyhole Tungsten Inert Gas welded joints*, Materials, 12(10), 1638
4. Tomków, J., Janeczek, A., Rogalski, G., Wolski, A., 2020, *Underwater local cavity welding of S460N steel*, Materials, 13(23), 5535.
5. Surojo, E., Aji, R.P., Triyono, T., Budiana, E.P., Prabowo, A.R., 2021, *Mechanical and microstructure properties of A36 marine steel subjected to underwater wet welding*, Metals, 11(7), 999.
6. Klett, J., Mattos, I.B.F., Maier, H.J., Silva, R.H.G., Hassel, T., 2020, *Control of the diffusible hydrogen content in different steel phases through the targeted use of different welding consumables in underwater wet welding*, Materials and Corrosion, 72, pp. 504-516.
7. Łabanowski, J., Prokop-Strzelczyńska, K., Rogalski, G., Fydrych, D., 2016, *The effect of wet underwater welding on cold cracking susceptibility of duplex stainless steel*, Advances in Materials Science, 16(2), pp. 68-77.
8. Xing, C., Jia, C., Han, Y., Dong, S., Yang, J., Wu, C., 2020, *Numerical analysis of the metal transfer and welding arc behaviors in underwater flux-cored arc welding*, International Journal of Heat and Mass Transfer, 153, 119570.
9. Wu, J., Han, Y., Jia, C., Wu, C., Yang, Q., 2020, *Underwater pulse-current FCAW – part 2: Bubble behaviors and waveform optimization*, Welding Journal, 99, pp. 303-311.
10. Parshin, S.G., 2021, *Underwater wet FCA-welding of high-strength steel X70 through the use of flux-cored electrode*, Welding International, 34, pp. 24-28.

11. Tomków, J., 2021, *Weldability of underwater wet-welded HSLA steel: Effect of electrode hydrophobic coatings*, Materials, 14(6), 1364.
12. Xu, C., Guo, N., Zhang, X., Chen, H., Fu, Y., Zhou, L., 2020, *Internal characteristic of droplet and its influence on the underwater wet welding process stability*, Journal of Materials Processing Technology, 280, 116593.
13. Wang, J., Sun, Q., Zhang, T., Tao, X., Jin, P., Feng, J., 2019, *Arc stability indexes evolution of ultrasonic wave-assisted underwater FCAW using electrical signal*, International Journal of Advanced Manufacturing Technology, 103, pp. 2593-2608.
14. Parshin, S.G., Levchenko, A.M., Maystro, A.S., 2020, *Metallurgical morel of diffusible hydrogen and non-metallic slag inclusions in underwater wet welding of high-strength steel*, Metals, 10(11), 1498.
15. Park, H., Moon, B., Moon, Y., Kang, N., 2021, *Hydrogen stress cracking behavior in dissimilar welded joints of duplex stainless steel and carbon steel*, Metals, 11(7), 1039.
16. Fydrych, D., Łabanowski, J., 2015, *An experimental study of high-hydrogen welding process*, Revista de Metalurgia, 51(4), e055.
17. Klett, J., Wolf, T., Maier, H.J., Hassel, T., 2020, *The applicability of the standard DIN EN SO 3690 for the analysis of diffusible hydrogen content in underwater wet welding*, Materials, 13(17), 3750.
18. Zavdoveev, A., Rogante, M., Poznyakov, V., Heaton, M., Acquier, P., Km, H.S., Baudin, T., Kostin, V., 2020, *Development of the PC-GMAW welding technology for TMCP steel in accordance with welding thermal cycle, welding technique, structure, and properties of welded joints*, Reports in Mechanical Engineering, 1(1), pp. 26-33.
19. Fydrych, D., Łabanowski, J., Rogalski, G., Haras, J., Tomków, J., Świerczyńska, A., Jakóbczak, P., Kostro, Ł., 2014, *Weldability of S500MC steel in underwater conditions*, Advances in Materials Science, 14(2), pp. 37-45.
20. Tomków, J., Janeczek, A., 2020, *Underwater in situ local heat treatment by additional stitches for improving the weldability of steel*, Applied Sciences, 10(5), 1823.
21. Adumane, S., Khan, G., Adedigba, S., Zendehboudi, S., 2021, *Offshore system safety and reliability considering microbial influenced multiple failure modes and their interdependencies*, Reliability Engineering & System Safety, 215, 107862.
22. Ali, L., Khan, S., Bashaml, S., Iqbal, N., Dai, W., Bai, Y., 2021, *Fatigue crack monitoring of T-type joints in steel offshore oil and gas jacket platform*, Sensors, 21(9), 3294.
23. Carpenter, K.R., Dissanayaka, P., Sterjovski, Z., Li, H., Donato, J., Gazder, A.A., van Duin, S., Miller, D., Johansson, M., 2021, *The effects of multiple repair welds on a quenched and tempered steel for naval vessel*, Welding in the World.
24. Qiang, X., Bijlaard, F.S.K., Kolstein, H., 2013, *Post-fire performance of very high strength steel S960*, Journal of Constructional Steel Research, 80, pp. 235-242.
25. Mician, M., Winczek, J., Harmaniak, D., Konar, T., Gucwa, M., Moravec, J., 2021, *Physical simulation of individual heat-affected zones in S960MC steel*, Archives of Metallurgy and Materials, 66(1), pp. 81-89.
26. Guo, W., Li, L., Dong, S., Crowther, D., Thompson, A., 2017, *Comparison of microstructure and mechanical properties of ultra-narrow gap laser and gas-metal-arc welded S960 high strength steel*, Optics and Lasers in Engineering, 91, pp. 1-15.
27. Ghafouri, M., Ahn, J., Mourujarvi, J., Bjork, T., Larkiola, J., 2020, *Finite element simulation of welding distortions in ultra-high strength steel S960 MC including comprehensive thermal and solid-state phase transformation models*, Engineering Structures, 219, 1100804.
28. Su, A., Liang, Y., Zhao, O., 2021, *Experimental and numerical studies of S960 ultra-high strength steel welded I-section columns*, Thin-Walled Structures, 159, 107166.
29. Sasikumar, A., Gopi, S., Mohan, D.G., 2021, *Effect of welding speed on mechanical properties and corrosion resistance rates of filler induced friction stir welded AA6082 and AA5052 joints*, Materials Research Express, 8, 066531.
30. Balamurugan, M., Gopi, S., Mohan, D.G., 2021, *Influence of tool pin profiles on the filler added friction stir spot welded dissimilar aluminium alloy joint*, Materials Research Express, 8, 096531.
31. Mician, M., Harmaniak, D., Novy, F., Winczek, J., Moravec, J., Trsko, L., 2020, *Effect of the t8/5 cooling time on the properties of S960MC steel in the HAZ of welded joints evaluated by thermal physical simulations*, Metals, 10(2), 229.
32. Szymczak, T., Szczucka-Lasota, B., Węgrzyn, T., Łazarz, B., Jurek, A., 2021, *Behavior of weld to S960MC high strength steel from joining process at micro-jet cooling with critical parameters under static and fatigue loading*, Materials, 14(11), 2707.
33. Schaupp, T., Rhode, M., Yahyanoui, H., Kannengieser, T., 2020, *Hydrogen-assisted cracking in GMA welding of high-strength structural steels using the modified spray arc process*, Welding in the World, 63, pp. 1997-2009.

34. Schaupp, T., Ernst, W., Spindler, H., Kannengieser, T., 2020, *Hydrogen-assisted cracking of GMA welded 960 MPa grade high-strength steels*, International Journal of Hydrogen Energy, 45(38), pp. 20080-20093.
35. Schaupp, T., Schroeder, N., Schroepfer, D., Kannengiesser, T., 2021, *Hydrogen-assisted cracking in GMA welding of high-strength structural steel – a new look into this issue at narrow groove*, Metals, 11(6), 904.
36. Wang, J., Sun, Q., Ma, J., Jin, P., Sun, T., Feng, J., 2016, *Correlation between wire feed speed and external mechanical constraint for enhanced process stability in underwater wet flux-cored arc welding*, Proceedings of the Institution of Mechanical Engineers Part B Journal of Engineering Manufacture, 233(6), pp. 1-13.
37. Tomków, J., Świerczyńska, A., Landowski, M., Wolski, A., Rogalski, G., 2021, *Bead-on-plate underwater wet welding of S700MC steel*, Advances in Science and Technology Research Journal, 15(3), pp. 288-296.
38. Tomków, J., Sobota, K., Krajewski, S., 2020, *Influence of tack welds distribution and welding sequence on the angular distortion of TIG welded joint*, Facta Universitatis-Series Mechanical Engineering, 18(4), pp. 611-621.
39. Kurc-Lisiecka, A., Lisiecki, A., 2017, *Laser welding of the new grade of advanced high-strength steel Domex 960*, Materiali in Tehnologije/Materials and Technology, 51(2), pp. 199-204.
40. Wang, J., Ma, J., Liu, Y., Zhang, T., Wu, S., Sun, Q., 2020, *Influence of heat input on microstructure and corrosion resistance of underwater wet-welded E40 steel joints*, Journal of Materials Engineering and Performance, 29, pp. 6987-6995.